Available online at www.sciencedirect.com
SCIENCE DIRECT®
International Journal of Heat and Fluid Flow 24 (2003) 538–550
International Journal of HEAT AND FLUID FLOW
www.elsevier.com/locate/ijhff

The inner–outer layer interface in large-eddy simulations with wall-layer models

Ugo Piomelli [a,*], Elias Balaras [a], Hugo Pasinato [b], Kyle D. Squires [b], Philippe R. Spalart [c]

[a] Department of Mechanical Engineering, University of Maryland, College Park, Maryland, MD 20742-3035, USA
[b] Department of Mechanical and Aerospace Engineering, Arizona State University, Tempe, AZ 85287, USA
[c] Boeing Commercial Airplanes, Seattle, WA 98124, USA

Received 23 November 2002; accepted 12 March 2003

Abstract

The interaction between the inner and outer layer in large-eddy simulations (LES) that use approximate near-wall treatments is studied. In hybrid Reynolds-averaged Navier–Stokes (RANS)/LES models a transition layer exists between the RANS and LES regions, which has resulted in incorrect prediction of the velocity profiles, and errors of up to 15% in the prediction of the skin friction. Several factors affect this transition layer, but changes we made to the formulation had surprisingly little effect on the mean velocity. In general, it is found that the correct prediction of length- and time-scales of the turbulent eddies in the RANS region is important, but is not the only factor affecting the results. The inclusion of a backscatter model appears to be effective in improving the prediction of the mean velocity profile and skin-friction coefficient.

PACS: 47.27.Eq; 47.27.Nz; 47.60.+i

1. Introduction

Large-eddy simulation (LES), a technique in which only the largest turbulent eddies are computed accurately, while the small ones are modeled, is increasizngly used as a tool to study turbulent flow problems for configurations in which the Reynolds-averaged Navier–Stokes (RANS) equations are not sufficiently accurate. Such problems include non-equilibrium, three-dimensional flows, relaminarizing and retransitioning boundary layers, and massively separated flows, especially if the sound emission is of concern. The fact that much of the energy is resolved, while only the smaller, more universal, eddies are modeled, results in significant advantages, in terms of accuracy, over the RANS approach. Since the grid size only needs to be small enough relative to the integral scale of motion, and does not need to match the Kolmogorov scales, LES is also significantly cheaper than direct numerical simulation (DNS) of the equations of motion.

Developments in modeling, numerical algorithms and computational speed have made it possible to apply LES to fairly complex problems at Reynolds numbers higher than those achievable by DNS. The application of LES has been particularly successful in non-equilibrium flows at moderate Reynolds numbers, in free-shear layers, and in massively separated flows in which the accurate simulation of regions near solid boundaries is not of primary importance. In massively separated flows, for instance, the detached-eddy simulation (DES) method, proposed by Spalart et al. (1997) (a hybrid technique in which the attached boundary layers are simulated using the RANS approach, while only the separated-flow zone is computed using LES) has had notable success. The main limitation of LES to date (in the absence of chemistry and/or multiple phases) appears to be in the application to high Reynolds-number boundary layers.

In these flows the advantage of LES, as it has generally been practiced, over DNS becomes less significant. Away from solid boundaries, the requirement that the energy-carrying scales of motion are resolved results in a grid size proportional to the integral scale of motion. Since this is usually a weak function of the Reynolds number (for the outer region of a turbulent boundary

* Corresponding author. Tel.: +1-301-405-2410; fax: +1-301-314-9477.
E-mail address: ugo@eng.umd.edu (U. Piomelli).

0142-727X/03/$ - see front matter © 2003 Elsevier Science Inc. All rights reserved.
doi:10.1016/S0142-727X(03)00048-1

layer, for instance, $\delta/c \sim Re^{-0.2}$ where c is the airfoil chord or other global dimension) the cost of LES does not depend strongly on the Reynolds number itself. If the near-wall region of a boundary layer needs to be resolved, on the other hand, the grid must be proportional to the size of the inner-layer eddies, which is strongly Reynolds-number dependent. Chapman (1979) estimated that the number of points required to resolve the wall layer is approximately

$$N_{xyz} \propto Re_L^{1.8}. \quad (1)$$

We use the short-cut notation N_{xyz} for the number of points in three dimensions, but observe that this estimate applies to grids made of nested and optimized layers, which coarsen as soon as possible away from the wall. Simple single-block structured grids would lead to worse scaling laws. In contrast, if designed according to the same principles, modern unstructured grids would have the same N_{xyz}.

This scaling, although more favorable than that of DNS

$$N_{xyz} \propto Re_L^{2.2}, \quad (2)$$

Reynolds (1990) still makes the resolution of the wall layer in high Reynolds-number flows infeasible with LES. Reynolds assumed single-block structured grids, which do not take full advantage of the easing resolution requirements as the distance from the wall increases (these grids coarsens only in the normal direction). However, this makes much less difference for a DNS than for an LES. The reason is that the Kolmogorov length scale grows relatively slowly, like the wall distance to the power 1/4 (because the dissipation drops like the inverse of the wall distance); in contrast, the size of the large eddies grows linearly with wall distance, so that a natural LES grid spacing also grows linearly.

To circumvent the high cost incurred to represent accurately the near-wall eddies, one can bypass the wall layer altogether, and model the effects of the eddies (small and large) present in this region in a statistical sense. Modeling the wall layer makes the number of grid points required by the calculation of a boundary layer proportional to $Re^{0.4}$ only (the resolution of each "cube of boundary-layer" requires a set number of points, but the cubes become more numerous as the Reynolds-number increase thins the boundary layer). However, this process re-introduces strong empiricism, for instance embodied in the express assignation of the value of the von Kármán constant κ. Two reassuring facts are that the empiricism is very stable in the sense that the near-wall region is very well known quantitatively, at least in equilibrium flows, and that grid refinement shrinks the region in which the empiricism is in control. Still, the rate at which modeling errors vanish is much less favorable than for free-shear flows.

Recent reviews of wall-layer models can be found in Cabot and Moin (2000) and Piomelli and Balaras (2002). Here, only a brief summary will be given. In general, wall-layer models (also known as "approximate boundary conditions") can be of two types: equilibrium laws and zonal models. Equilibrium laws assume that the dynamics of the wall-layer are universal and that some generalized law-of-the-wall exists (at least if the equations are averaged over a large enough patch); the wall stress is then computed from this general law, which is applied some distance away from the wall. Their RANS equivalent are "wall functions". Although equilibrium laws have been used with considerable success in simple, attached flows (especially in meteorological applications), they suffer from significant limitations. They cannot be applied easily in complex geometries, on fully-unstructured grids, or in flows in which the mean velocity profile is not known a priori even very close to the wall. For instance, in calculations of the flow in a rotating channel, equilibrium laws could not predict the quasi-relaminarization that is observed on one side of the channel (Balaras et al., 1996). Thus, their value as a predictive tool in engineering applications is limited.

Zonal approaches are hybrid RANS/LES methods that solve the filtered Navier–Stokes equations away from the wall, and the unsteady RANS (URANS) equations in the near-wall region. The simulation extends to the wall, where the no-slip condition is applied. Zonal approaches are based on the explicit solution of a different set of equations in the inner layer; still, a field equation is used rather than a single relation between stress and velocity at the wall-layer edge. Two techniques of this type have been used up to now: in the first, known as the "two-layer model" (TLM) two separate grids are used, while in the other, which is based on the DES method, a single grid is used, and only the turbulence model changes from one region to the other.

The TLM was proposed by Balaras and Benocci (1994) and Balaras et al. (1996). While the filtered Navier–Stokes equations are solved in the core of the flow, in the wall-layer a simplified set of equations is solved in a fine grid embedded under the coarser, LES, mesh. The cost of this method is marginally higher than the cost of calculations that use equilibrium boundary-conditions, since the inner layer, despite the fact that is discretized using a very fine grid in the normal direction, requires a small percentage of the total cost of the calculation: two one-dimensional problems are solved, and no Poisson-equation inversion is required to obtain the pressure. This method has been used in channel flow at high Reynolds numbers (Balaras et al., 1996), backward-facing steps (Cabot, 1996; Diurno et al., 2001), and in calculations of the trailing edge of an airfoil (Wang and Moin, 2002), with fairly accurate results.

DES was introduced by Spalart et al. (1997) as a method to compute massively separated flows. DES is a hybrid approach that combines the solution of the RANS equations in the attached boundary-layers with the solution of the LES equations in the separated regions, which are where the detached eddies are important. Because the governing equations must be integrated in a time-accurate fashion in DES, the "RANS region" is modeled via solution of the URANS equations. While the integration in time of the RANS equations is straightforward in practice, the interpretation of URANS is less obvious (see Spalart (2000) for additional discussion). DES possesses the advantage that, as in classical LES, grid and time-step refinements yield additional physics, i.e., an increased range of length and time scales are resolved. This is a very desirable attribute as the fine-grid limit of DES is a DNS for which empirical input via the turbulence model vanishes.

In the standard DES approach the entire boundary layer is modeled by URANS. Nikitin et al. (2000), however, used DES as a wall-layer model in calculations of plane channel flow. In their computations, in the inner layer the URANS equations were solved, with the Spalart and Allmaras (1994) model to parameterize the effect of all scales of motion. The Reynolds shear stress, in this region, was provided entirely by the turbulence model. In the outer flow the model was modified to yield a much lower eddy viscosity than it would as a pure RANS model, which allowed the formation of turbulent eddies capable of supporting most of the Reynolds shear stress. Nikitin et al. (2000) performed calculations with different numerical schemes and grids, exploring a wide range of Reynolds numbers ($180 \leqslant Re_\tau \leqslant 80{,}000$). The calculations showed some promising results: turbulence in the outer layer was sustained even though the grids were not particularly fine and the flow in the inner layer was, visually, too smooth (this was not shown by Nikitin et al. (2000), but was verified subsequently). The skin-friction coefficient C_f, however, was under-predicted by approximately 15% in most cases. At intermediate and high Reynolds numbers a logarithmic region with the correct intercept developed in the quasi-steady RANS region, that connected to an LES region characterized by an excessively high intercept of the logarithmic layer, which was reflected in the low values of C_f. Grid refinement translated this undesirable "step" towards the wall, but without changing its height. Furthermore, unphysical, very elongated wall streaks were formed in the RANS region.

Both these issues have been investigated by several researchers (Baggett, 1998; Piomelli et al., 2001; Hamba, 2002). Baggett (1998) argues that the DES buffer layer is due to the presence of the artificial streaks, which causes a de-correlation between streamwise and wall-normal fluctuations that must be compensated by a higher velocity gradient to balance streamwise momentum; as a result, the intercept of the LES logarithmic region is shifted to a higher value. Hamba (2002) performed simulations in which the inner layer was modeled by RANS, the outer by LES, and obtained the shift mentioned before; he then used RANS in the outer layer and LES in the inner one, with the same result.

Based on these findings, it appears that the shift in the logarithmic layer is quite robust, its appearance depending more on the grid resolution than on the modeling approach. The discrepancy between the log-law intercepts in the inner and outer layer is due to the transition between the LES and RANS regions. Here, the eddy viscosity is lower than if it were a RANS region, but the Reynolds-stress generating scales have not yet been formed; thus, the resolved motions cannot yet support their share of the shear stress, while the model has already switched to the LES mode; the only way to reach the equilibrium value of the shear stress (which, in the plane channel, is fixed by the distance from the wall) is by a velocity gradient increase that balances the eddy viscosity decrease.

Several ways to alleviate this problem have been proposed. Piomelli et al. (2001) investigated whether bringing the RANS/LES interface closer to the wall, or using less dissipative outer-layer SGS models, would facilitate the generation of Reynolds-stress generating structures. They found that the shift in the log layer was unaffected by these changes. Hamba (2002) had some success by prescribing an overlap zone in which the model switched smoothly from the RANS to the LES formulation. This zone extended to approximately 20% of the channel half-width. Other hybrid techniques that combine RANS and LES, while not applied as wall models to date, would suffer from similar errors without ad hoc adjustments being made to the underlying closure.

Another possible method is the use of a backscatter model in the inner layer. Several types of backscatter models have been used in LES (Leith, 1990; Chasnov, 1991; Carati et al., 1995), mostly within the framework of homogeneous flows. Mason and Thomson (1992), however, used stochastic backscatter in calculations of boundary layers at very high Reynolds numbers. They used approximate boundary conditions of the logarithmic type (Mason and Callen, 1986). Although in their calculations the inner layer was bypassed entirely, they also found a shift in the logarithmic region, with a higher velocity gradient at the first few grid points, that was corrected when the backscatter model was introduced. Baggett (1998) suggested that the stochastic backscatter had the effect of breaking up the "super-streaks" and thus introduce a de-correlation of the velocity that allowed a more rapid formation of Reynolds-stress generating eddies.

In the present paper we will examine these issues in more detail. In particular, we will describe the effects of

the interface location both on the turbulent statistics and on the turbulence structure. We will then propose and test the use of a backscatter model in the inner layer. In the following, the problem will first be set up, and the important equations will be presented. Then, the numerical results will be shown and discussed. Finally, some conclusions and recommendations for future work will be made.

2. Problem formulation

The problem used to study the interaction between RANS and LES zones is the plane channel flow. The filtered equations of conservation of mass and momentum

$$\frac{\partial \bar{u}_j}{\partial x_j} = 0, \tag{3}$$

$$\frac{\partial \bar{u}_i}{\partial t} + \frac{\partial}{\partial x_j}\left(\bar{u}_j \bar{u}_i\right) = -\frac{\partial \bar{p}}{\partial x_i} + \frac{1}{Re_\tau}\nabla^2 \bar{u}_i - \frac{\partial \tau_{ji}}{\partial x_j} \tag{4}$$

(where the over-bar denotes filtered variables and the effect of the subgrid scales appears through the SGS stresses $\tau_{ij} = \overline{u_i u_j} - \bar{u}_i \bar{u}_j$) are solved numerically using a second-order accurate finite-difference method on a staggered grid. The discretized equations are integrated in time using a semi-implicit fractional time-step method, in which the wall-normal diffusive terms are advanced in time using the Crank–Nicolson method, the remaining diffusive terms and the convective term are advanced using the Adams–Bashforth method. The Poisson equation is then solved using a direct solver, and the velocity is corrected to make the field solenoidal. The flow is driven by a pressure gradient that is varied in time in such a way as to maintain the mass flux through the channel constant.

In the DES approach the SGS stresses are parameterized using an eddy-viscosity model:

$$\tau_{ij} - \tfrac{2}{3}\delta_{ij}\tau_{kk} = -2\nu_T \overline{S}_{ij}, \tag{5}$$

$$\overline{S}_{ij} = \frac{1}{2}\left(\frac{\partial \bar{u}_i}{\partial x_j} + \frac{\partial \bar{u}_j}{\partial x_i}\right). \tag{6}$$

The eddy viscosity is obtained by solving a transport equation for an auxiliary variable $\tilde{\nu}$:

$$\frac{D\tilde{\nu}}{Dt} = c_{b1}\widetilde{S}\tilde{\nu} - c_{w1} f_w \left[\frac{\tilde{\nu}}{\widetilde{d}}\right]^2 + \frac{1}{\sigma}\left\{\nabla\cdot\left[(\nu+\tilde{\nu})\nabla\tilde{\nu}\right] + c_{b2}(\nabla\tilde{\nu})^2\right\} \tag{7}$$

in which the LHS contains the unsteady and advective terms, and the first group in the RHS is the production term, the second is a destruction term, the last one is a diffusion term. The other quantities in (7) are given by:

$$\widetilde{S} = |\overline{S}| + \frac{\tilde{\nu}}{\kappa^2 \widetilde{d}^2} f_{v2}, \quad f_{v1} = \frac{\chi^3}{\chi^3 + c_{v1}^3},$$

$$f_{v2} = 1 - \frac{\chi}{1 + \chi f_{v1}},$$

$$\nu_T = \tilde{\nu} f_{v1}, \quad \chi \equiv \frac{\tilde{\nu}}{\nu}, \quad f_w = g\left[\frac{1 + c_{w3}^6}{g^6 + c_{w3}^6}\right]^{1/6},$$

$$g = r + c_{w2}(r^6 - r), \quad r \equiv \frac{\tilde{\nu}}{\widetilde{S}\kappa^2 \widetilde{d}^2},$$

where $|\overline{S}| = (2\overline{S}_{ij}\overline{S}_{ij})^{1/2}$, $\widetilde{d}$ is the minimum between the RANS and LES length scales, and $\widetilde{d} = \min(d_{RANS}, d_{LES})$; its definition and role will be discussed later. The constants are:

$$c_{b1} = 0.1355, \quad \sigma = 2/3, \quad c_{b2} = 0.622, \quad \kappa = 0.41,$$

$$c_{w1} = c_{b1}/\kappa^2 + (1 + c_{b2})/\sigma,$$

$$c_{w2} = 0.3, \quad c_{w3} = 2.0, \quad c_{v1} = 7.1.$$

The model constants have been evaluated using several building block flows (Spalart and Allmaras, 1994). The use of $\tilde{\nu}$ instead of the eddy viscosity is motivated by the fact that, unlike ν_T, the new variable behaves linearly near the wall and does not require the use of damping functions. In the present simulations, (7) is discretized on the same grid as the pressure (i.e., the eddy viscosity is located at the pressure points), and is integrated in time using a semi-implicit method. The non-linear terms on the RHS are evaluated partly at the new time-step, partly at the old one (for instance, the second part of the diffusion term is written as $c_{b2}\nabla\tilde{\nu}^{n+1}\nabla\tilde{\nu}^n$). All terms are then integrated using an implicit Crank–Nicolson method, except for the advection, which is advanced in time using the Adams–Bashforth scheme.

All calculations were carried out using a domain whose dimensions are $2\pi\delta \times \pi\delta \times 2\delta$ in the streamwise, spanwise and wall-normal directions (x, y and z, respectively); δ is the channel half-height. The Reynolds number (based on friction velocity and channel half-width) was approximately equal to 5000. The same grid spacing was used for all calculations in the planes parallel to the wall: $\Delta x = \Delta y = 0.049\delta$. This value satisfies theoretical estimates (Chapman, 1979) and previous calculations (Nikitin et al., 2000), which indicate that between 15 and 20 points per channel half-height are required to resolve accurately the outer-layer structures. The mesh in the wall-normal direction is stretched using a hyperbolic tangent transformation. The first grid point is always maintained at $z^+ < 1$, and the maximum grid spacing in the wall-normal direction is $\Delta z_{max} = 0.054\delta$. This results in nearly cubic grid cells in the outer flow, and very flat cells in the near-wall region. This is a requirement of DES, and is not a general one for LES near-wall treatments. It increases the cost trend as a

function of Re, but only moderately; the cost, in fact, only increases logarithmically (Nikitin et al., 2000).

When the Spalart and Allmaras model (1994) (which in the following will be referred to as "SA model") is used either for DES or as a wall model, the length-scale $\widetilde{d}$ plays a crucial role. In wall-modeling applications, the RANS length scale d_{RANS} is taken to be the distance from the wall, z_{w}. At a distance from the wall z_{switch} (the point where $z_{\mathrm{w}} = d_{\mathrm{LES}}$), the length scale $\widetilde{d}$ switches from the RANS-like length scale (the distance from the wall) to an LES-like one, d_{LES} (the filter width, which is typically related to the grid size). As a consequence, the "destruction of eddy-viscosity" term is increased, and the eddy viscosity has smaller values than expected when the model is used for RANS. In the present investigation, d_{LES} was given by

$$d_{\mathrm{LES}} = C_{\mathrm{DES}}\Delta. \tag{8}$$

Two forms of Δ were used in this work: the original one proposed by Nikitin et al. (2000) is

$$\Delta = \max(\Delta x, \Delta y, \Delta z). \tag{9}$$

The relation (9) does not account for the shape of the grid cells and leads to a constant filter width in the LES region (Fig. 1). An alternative form of Δ is also employed in the present computations,

$$\Delta = C_{\mathrm{DES}}(\Delta x^2 + \Delta y^2 + \Delta z^2)^{1/2}. \tag{10}$$

This expression, unlike (9), accounts for factors such as the grid-cell aspect ratio. Powers higher than two can be used and approach the original definition. If the value of C_{DES} is unchanged, the definition (10) is larger than (9) by a factor of approximately $\sqrt{2}$ near the wall, and $\sqrt{3}$ at the center of the channel (Fig. 1).

To examine the effect of z_{switch}, various values of C_{DES} were tested. In the present calculations, the switch occurs between $0.045\delta \geqslant z_{\mathrm{switch}} \geqslant 0.018\delta$ (depending on the value of C_{DES}), which correspond to $225 \geqslant z^+_{\mathrm{switch}} \geqslant 90$. At this location the model smoothly evolves from a RANS-like model to an LES-like one, and the blending region mentioned above is expected to be found. The length-scales corresponding to the values of C_{DES} used are shown in Fig. 1, and a summary of the calculations can be found in Table 1.

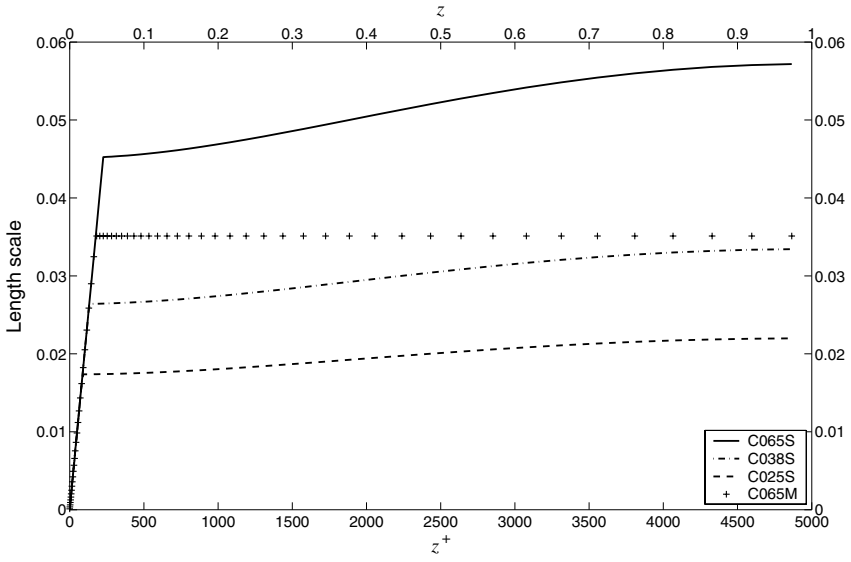

Fig. 1. Length scales for the DES calculations.

Table 1
Summary of computational parameters

Case	C_{DES}	Δ	z_{switch}	z^+_{switch}	Model inner/outer
C065S	0.65	$(\Delta x^2 + \Delta y^2 + \Delta z^2)^{1/2}$	0.046	225	SA/SA
C038S	0.38	$(\Delta x^2 + \Delta y^2 + \Delta z^2)^{1/2}$	0.027	112	SA/SA
C025S	0.25	$(\Delta x^2 + \Delta y^2 + \Delta z^2)^{1/2}$	0.018	90	SA/SA
C038Smag	0.38	$(\Delta x^2 + \Delta y^2 + \Delta z^2)^{1/2}$	0.027	112	SA/Smag
C065M	0.65	$\max(\Delta x, \Delta y, \Delta z)$	0.036	180	SA/SA
C065Mλ	0.65	$\max(\Delta x, \Delta y, \Delta z)$	0.036	180	SA/SA + forcing
C065MB	0.65	$\max(\Delta x, \Delta y, \Delta z)$	0.036	180	SA/SA + forcing

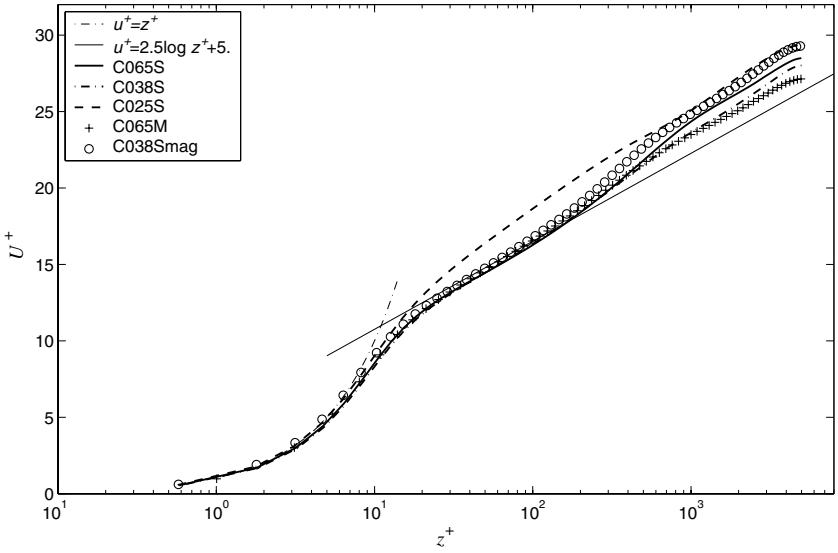

Fig. 2. Mean velocity profiles.

3. Results and discussion

When the DES approach is used with the standard value $C_{\mathrm{DES}} = 0.65$, Fig. 2, the step in the profile reported by Nikitin et al. (2000) is clearly visible. The error in the prediction of the skin-friction coefficient is 16.5% or 22.1%, depending on whether Δ is defined by (9) or (10). The velocity profile has the correct behavior in the inner layer, which is governed by the RANS model, tuned to reproduce the linear and logarithmic profiles in flows of this kind. As the flow transitions into the LES region, however, an unphysical "DES buffer layer" is formed in which the velocity gradient $\mathrm{d}U/\mathrm{d}z$ is too high. A new logarithmic region can then be observed with a high intercept. The error in the prediction of the skin friction coefficient is defined as

$$\mathrm{Error} = \frac{|C_{\mathrm{f}} - C_{\mathrm{f,Dean}}|}{C_{\mathrm{f,Dean}}} \times 100, \tag{11}$$

where the C_{f} is

$$C_{\mathrm{f}} = \frac{\tau_{\mathrm{w}}}{\rho U_{\mathrm{b}}^2/2}; \tag{12}$$

here, $\tau_{\mathrm{w}} = \mu \mathrm{d}U/\mathrm{d}z|_{\mathrm{w}}$ is the mean wall stress, U_{b} is the average velocity in the channel, and

$$C_{\mathrm{f,Dean}} = 0.073 Re_{\mathrm{b}}^{-1/4} \tag{13}$$

(Dean, 1978), with $Re_{\mathrm{b}} = 2U_{\mathrm{b}}\delta/\nu$ (where δ is the channel half-width). The percent error for all the simulations is reported in Table 2.

Time histories of the streamwise velocity are shown in Fig. 3. The velocity in the inner layer and in the blending layer is smooth, and the smallest timescale present in the flow is of order $0.3\delta/u_\tau$. Only for $z^+ > 2000$ are shorter timescales generated. In addition, we observe a strong vertical correlation between the time-series for $z^+ < 1000$, which can be observed in the spatial structures as well (see below).

"Super-streaks" can be observed in the velocity-fluctuation contours (Fig. 4). In the RANS region ($z^+ < z^+_{\mathrm{switch}} = 225$) the flow is not entirely smooth: significant fluctuation levels exist, but the size of the eddies in this region is unphysical. Also, one can observe a strong correlation between the velocity fields for $z^+ < 1500$. Only above this value shorter-scale eddies are formed, and the more isotropic eddies that are expected in the outer flow can be observed.

Zonal approaches employ parameterizations in the near-wall layer based on equilibrium, i.e., these approaches presume that the timescales of the inner-layer structures τ_{inn} are much shorter than the timescales associated with outer-layer eddies, $\tau_{\mathrm{out}} \sim 1/|\overline{S}|$. The small inner-layer eddies are, however, smoothed by the spatial grid-averaging, and by the temporal filtering implicitly applied by the use of a time-step that is of the same

Table 2
Percent error in the prediction of the skin friction coefficient C_{f}

Case	C065S	C038S	C025S	C038Smag	C065M	C065Mλ	C065MB
% Error	22.1	19.0	27.6	25.7	16.5	5.3	11.2

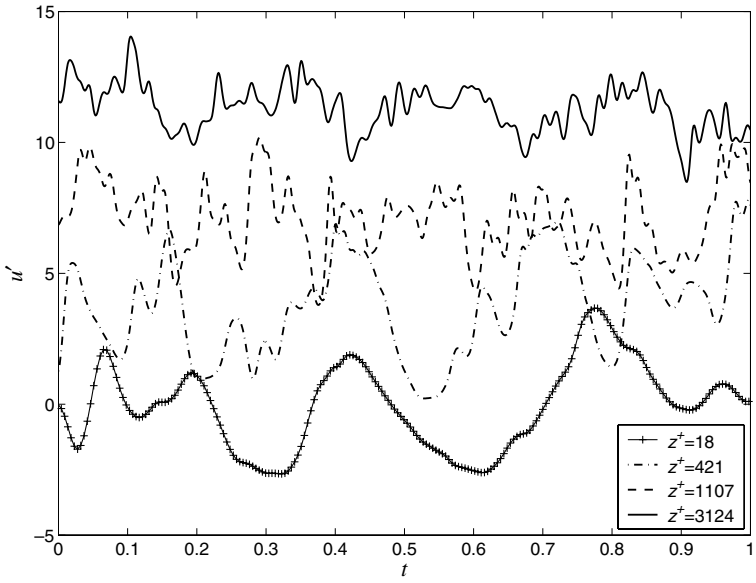

Fig. 3. Time-histories of the velocity. Run C065S.

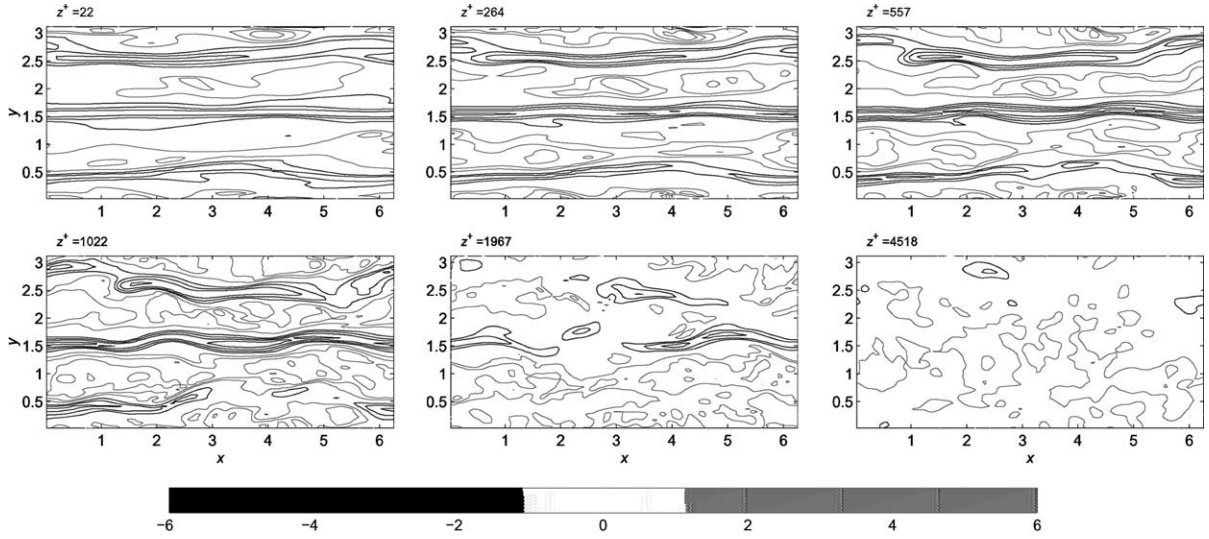

Fig. 4. Contours of streamwise velocity fluctuations in planes parallel to the wall. Run C065S.

order as τ_{out}. As a result of the modeling assumptions, then, the inner-layer flow should have the same time-scale as the outer flow, τ_{out}. The SA model, however, tends to smooth the velocity significantly in the inner layer, and the time-scales there are considerably longer than the outer-layer ones. This is not natural, and it makes a poor use of the resolution in both space and time for the wall region, which is crucial. In the outer layer, where the eddy viscosity is decreased and the elongating effect of the mean shear is much weaker, shorter time-scales are generated; the DES buffer is the region in which these scales are formed.

Decreasing the value of C_{DES} is only partially beneficial. When the RANS/LES transition is brought closer to the wall, smaller scales are indeed generated (Fig. 5). The velocity fluctuation contours still show very elongated structures, but their streamwise extent is significantly reduced. Eddies with shorter wavelengths and time-scales can be observed even relatively close to the wall (starting from the second level shown in the plots, $z^+ = 256$), and the physical picture of the blending region becomes more similar to what is expected. However, the "DES buffer layer" is not eliminated, merely shifted closer to the wall (Fig. 2). The errors in the skin friction prediction, reported in Table 2, remained significant.

The results obtained using $C_{DES} = 0.65$ and $\Delta = \max(\Delta x, \Delta y, \Delta z)$ (Case C065M), or $C_{DES} = 0.38$ and the

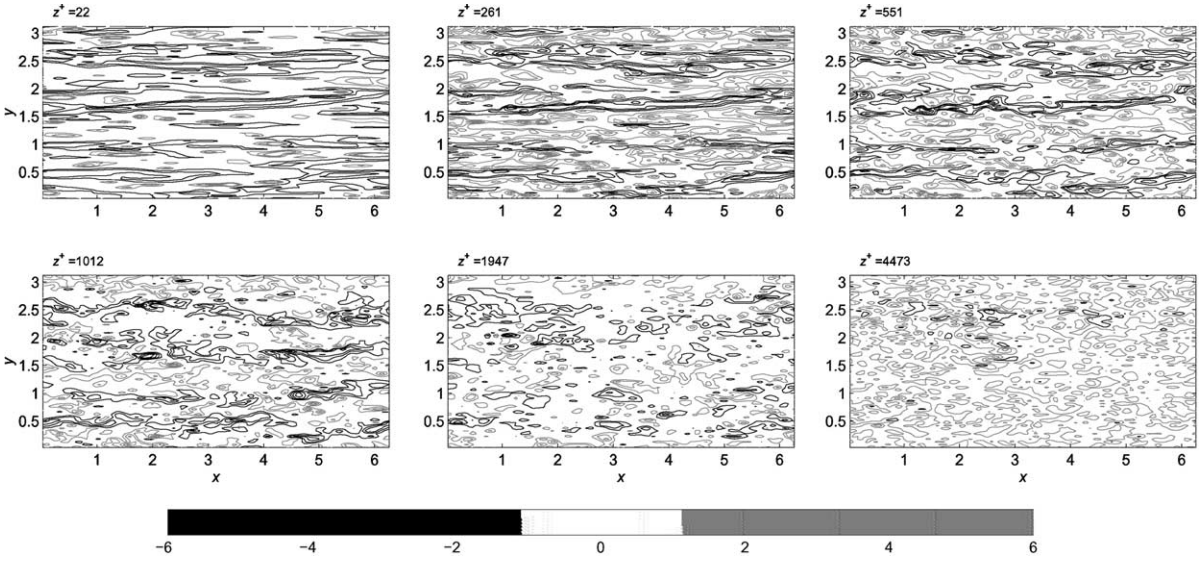

Fig. 5. Contours of streamwise velocity fluctuations in planes parallel to the wall. Run C038S.

square-root definition of Δ (Case C038S) were very similar (see Fig. 2); this reflects the similarity of the length-scale distributions in these cases (Fig. 1). The use of $C_{\mathrm{DES}} = 0.65$ with the square-root definition results in excessively high values of the eddy viscosity (Fig. 6), especially for $100 < z^+ < 1000$. Worse results were obtained with $C_{\mathrm{DES}} = 0.25$. In this case, in fact, the switch between RANS and LES zones takes place at the lower edge of the logarithmic layer. As a result the entire logarithmic layer is displaced.

We also investigated whether coupling the inner-layer model to a different outer-layer model could be beneficial. To this end, the SA inner-layer model was matched with the Smagorinsky model, which is expected to be more responsive to the outer-layer velocity field. Although this modification significantly altered the eddy-viscosity distribution, which was much lower in the outer layer (Fig. 6), and was successful in introducing short-scale fluctuations, the shift in the logarithmic layers remains (compare with Fig. 2).

The fact that the structure of the flow can be modified significantly without affecting the mean velocity profile indicates that the coupling between the physical picture of the RANS/LES transition region and the mean velocity profile may be weaker than conjectured by (among others) Baggett (1998) and Piomelli and Balaras (2002). Lowering the interface did result in increased resolved stress in some regions (Fig. 7). In particular,

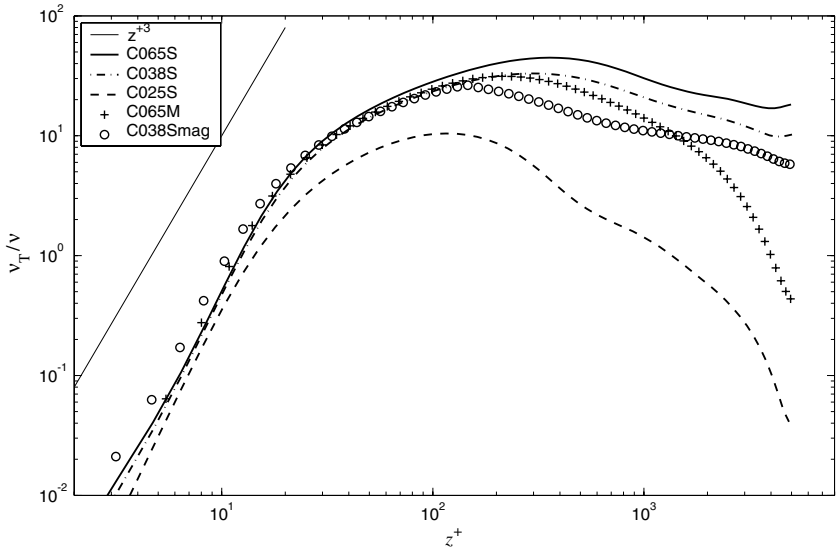

Fig. 6. Eddy-viscosity profiles.

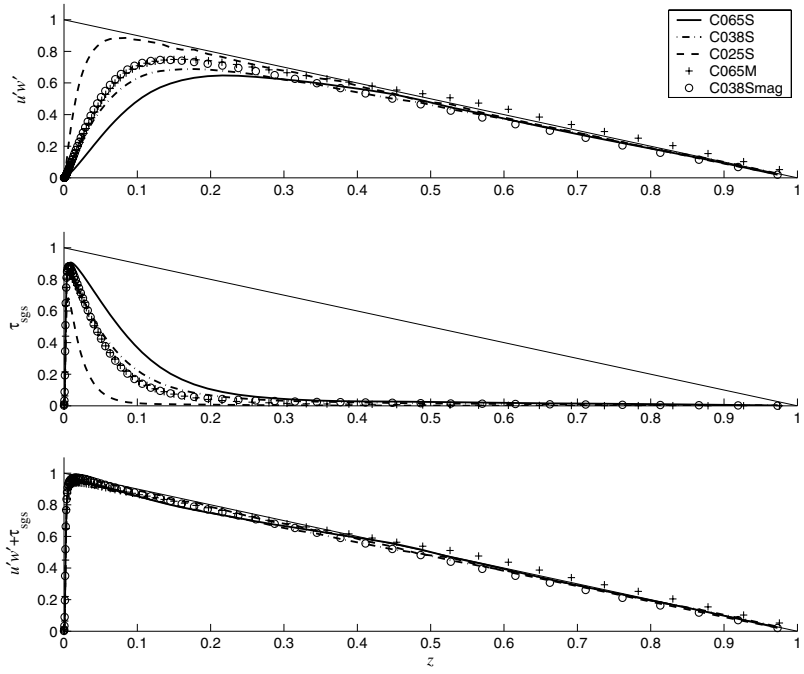

Fig. 7. Shear stress profiles: (a) resolved; (b) modeled; (c) total.

this indicates that the connection between the "super-streaks" and the increased velocity gradient is not very strong, and that small-scale structures can be generated near the wall by changing the location of the interface without altering the mean velocity profiles.

A further series of tests involved the use of a stochastic backscatter model in the inner layer. To this end a forcing term f_i was added to the right-hand-side of the momentum equation (4). A stochastic backscatter model has at least three free parameters: a length scale L_f, a characteristic time-scale T_f, and an amplitude. Since the backscatter represents the effect of subgrid-scales, its length scale should be the filter width, and its time-scale should be the time step. For these reasons, the forcing was obtained from a series of Gaussian random numbers, which were generated at each time-step. The amplitude of the forcing was designed to vanish at the walls, and be non-zero only over a thin layer, usually straddling the interface between LES and RANS regions. A typical amplitude envelope used in the simulations was

$$f(z) = A\frac{(\lambda z)^2}{1+(\lambda z)^4}; \tag{14}$$

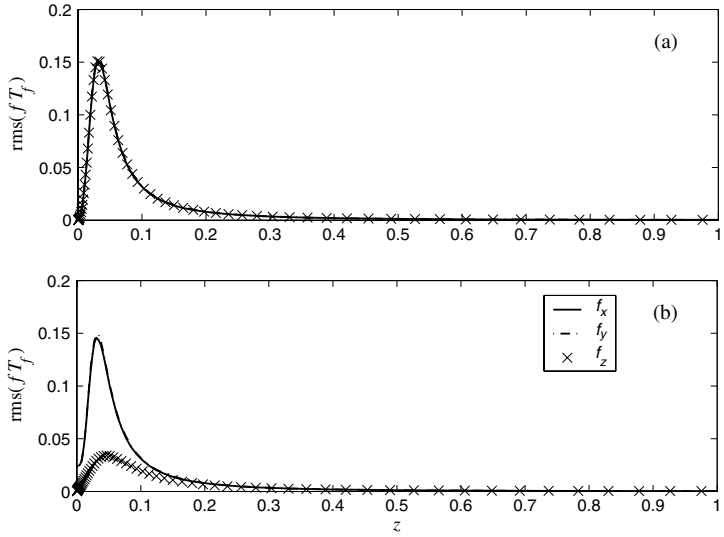

Fig. 8. Root-mean-square distributions of the forcing: (a) before the projection; (b) after the projection.

the peak of f occurs at $z \sim 1/\lambda$; a value of $\lambda = 30$ centers the function near the RANS/LES interface; A is an amplitude parameter that, in this work, was determined empirically. The force was filtered in all directions using a top-hat filter with filter-width equal to the grid spacing. Finally, the forcing was projected onto a divergence-free field, which was added to the right-hand-side of the Navier–Stokes equations. Root-mean square fluctuations of the force for a representative case (case C068Mλ) are shown in Fig. 8. Notice how the projection damps the wall-normal component of the forcing very significantly: the forcing does not affect directly the wall-normal transport of momentum as substantially as the other velocity components. The backscatter model proposed by Mason and Thomson (1992) has a similar distribution, but lower amplitude and a peak closer to the wall. Exponential envelopes were also tried (case C065MB, for instance) with similar distributions and, as will be shown, similar results. The maximum amplitude was varied over a significant range; low values of A

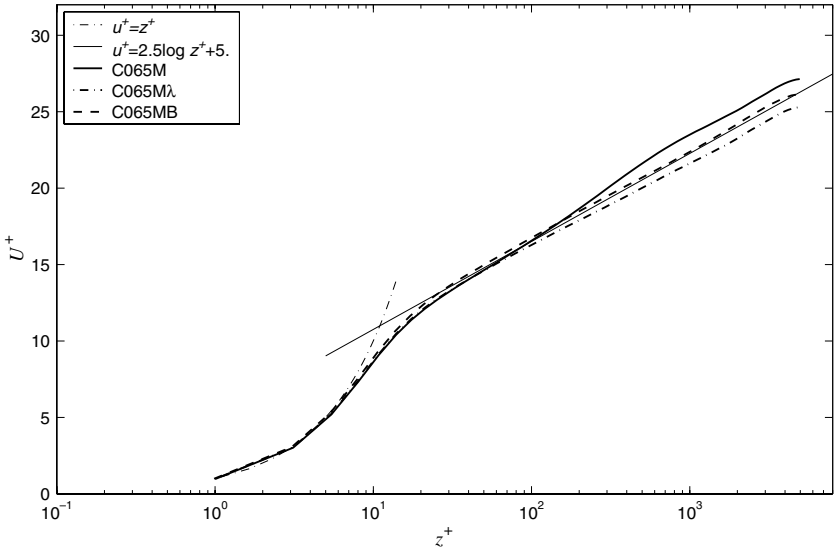

Fig. 9. Mean velocity profiles.

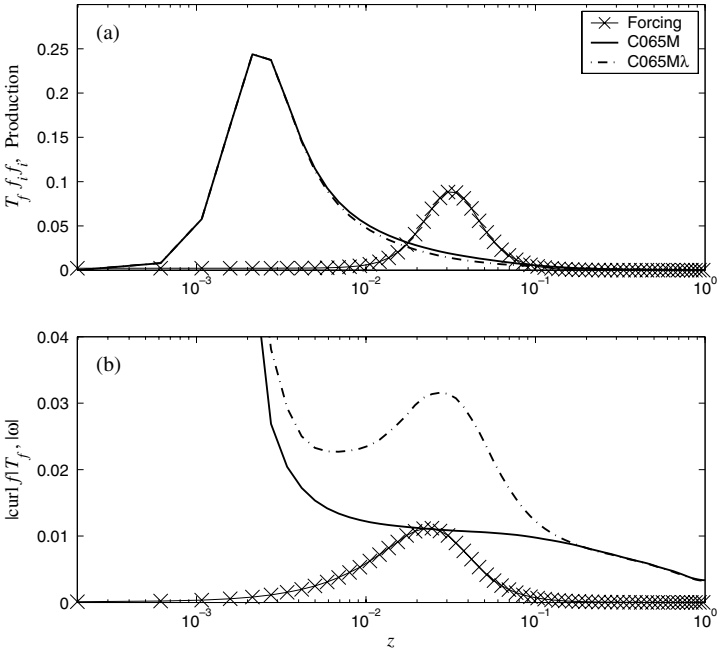

Fig. 10. (a) Energy input by the backscatter model compared with the turbulent kinetic energy production $-\langle u''w'' + \nu_T(\mathrm{d}u/\mathrm{d}z)\rangle(\mathrm{d}U/\mathrm{d}z)$; (b) magnitude of the curl of the stochastic force compared with the vorticity magnitude $(\omega_i'\omega_i')^{1/2}$. All quantities normalized by u_τ and ν.

resulted in little change in the mean velocity profile. Only the cases in which the mean velocity profile was modified will be shown here.

Fig. 9 shows the velocity profiles obtained using the backscatter models described above, with a case in which no stochastic forcing was used. A significant improvement in the mean velocity profile can be seen, which results in a nearly correct prediction of the skin-friction coefficient. The error, in fact, is reduced to approximately 5% in the C065Mλ case.

The backscatter model generated zero mean momentum; although a new set of random numbers was generated at each time step, to approximate white noise, the net energy input was non-zero due to the discrete implementation of the forcing. The forcing does, in fact, act for a finite time $T_f = \Delta t$; this produces a correlation between f_i at time-step n and the velocity u_i at time-step $n+1$. It can easily be shown that the rate of kinetic energy production due to the backscatter model is $T_f f_i f_i$ (e.g., see Eswaran and Pope, 1988). This quantity is compared in Fig. 10 with the turbulent kinetic energy production. The backscatter model inputs a significant amount of energy, only a factor of two lower than the peak energy production in the near-wall layer, and over a thicker layer.

In addition to the production of energy, the backscatter model also introduces vorticity. The magnitude of the curl of the stochastic forcing is compared in Fig. 10 with the fluctuating vorticity, both for a case with no backscatter, and for one with the stochastic forcing. The peak of the curl of the backscatter force occurs slightly below the RANS/LES interface, and also below the value where $f(z)$ peaks; this is due to the grid stretching near the wall, which results in higher vorticity (for a given amplitude of the forcing) in regions of grid refinement. The effect of the model is clearly to generate

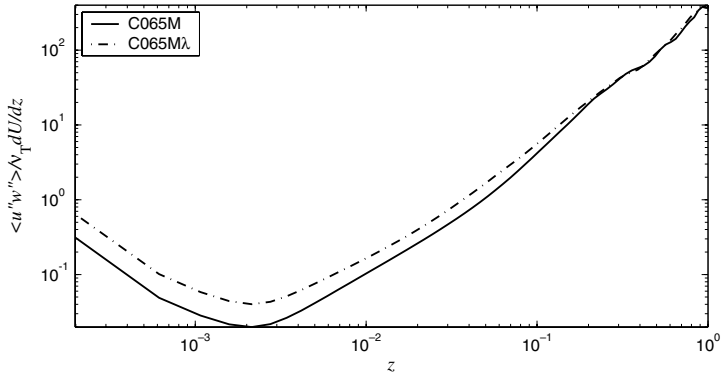

Fig. 11. Ratio of the resolved stresses, $\langle u''w'' \rangle$ to the modeled ones, $\nu_T \, dU/dz$.

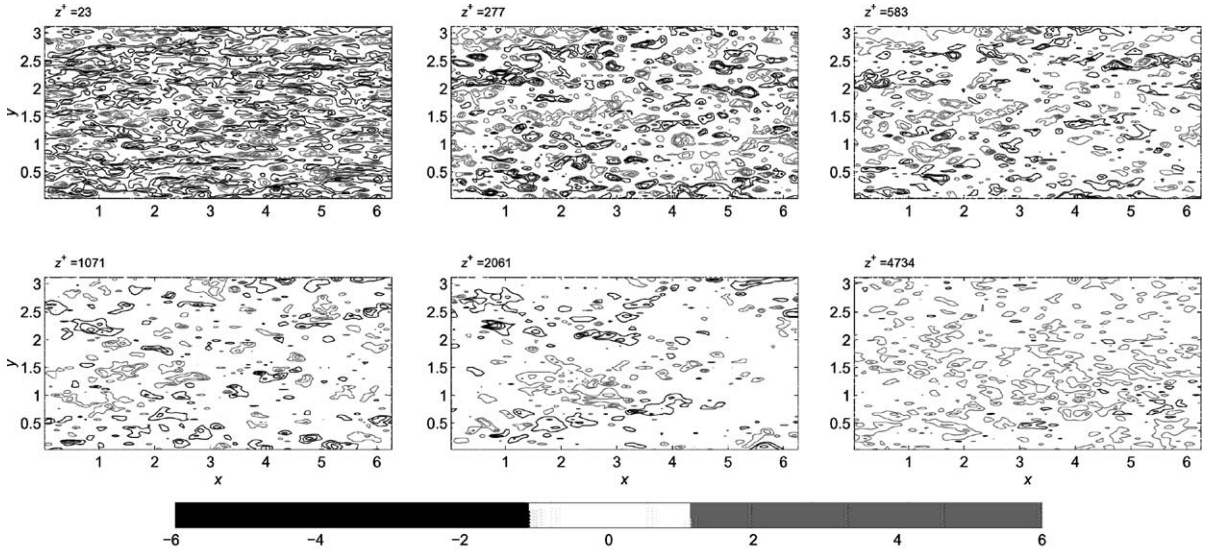

Fig. 12. Contours of streamwise velocity fluctuations in planes parallel to the wall. Run C065Mλ.

rotational motions that are effective in supporting Reynolds shear stress, thus altering the shear stress distribution and the mean velocity profile. Fig. 11 compares the ratio of the resolved stresses, $\langle u''w''\rangle$ to the modeled ones, $\nu_T \mathrm{d}U/\mathrm{d}z$, for two simulations, one including the backscatter model (case C065Mλ) and one without it (case C065M). It is quite clear that, when stochastic forcing is included, the eddies generated in the the near-wall region support a significantly higher proportion of the Reynolds shear stress. Notice that the forcing is uncorrelated: $\langle f_x f_z\rangle = 0$: the non-linear interactions between eddies generate the phase information responsible for the increased resolved stress below the RANS/LES interface.

Finally, Fig. 12 shows the streamwise velocity fluctuation contours in planes parallel to the wall for case C065Mλ. The introduction of the stochastic forcing has clearly been successful in breaking up the "superstreaks" and generating smaller scales near the interface.

4. Conclusions

We have studied the interaction between inner and outer regions in hybrid RANS/LES calculations in which the inner region is modeled by RANS methods, and the outer one using the LES approach. The hybrid approach has been found by many investigators to result in an unphysical transition between the two regions, which affects the accuracy of the prediction of the velocity profile and skin friction. This error is due to a mismatch of scales between RANS and LES regions: while in the RANS inner layer the turbulence model supports most of the Reynolds shear stress, in the LES region the resolved eddies must supply the dominant contribution. In the transition region the eddy-viscosity contribution to mean shear stress is too low, while energy-carrying eddies have not yet been generated. As a result, global balance of momentum can be ensured only by a higher velocity gradient in the transition region.

The location of the RANS/LES interface does not affect the results significantly: when it is lowered, despite the fact that shorter length-scales are generated, the ratio of resolved to modeled stress is affected, but not enough to correct the mean velocity profile. The introduction of a backscatter model based on stochastic forcing was successful. Forcing was performed only in the region immediately below the interface. Various amplitudes and envelopes of the stochastic forcing were tested, and it was found that when the energy input of the model was comparable to the turbulent kinetic energy production, Reynolds-stress carrying eddies could be generated. This resulted in improved prediction of the mean velocity profile and skin friction coefficients.

The present backscatter study should be viewed as a proof-of-feasibility: the model that we propose has no physical justification, at this point. Although its general behavior follows that of the model proposed by Mason and Thomson (1992), its amplitude is significantly larger than that proposed by those researchers. The demonstration that this method may be effective, however, suggests that renewed effort should be made to develop and test models of this type, and base them on sound physical arguments.

Acknowledgements

Supported by the Office of Naval Research under Grant No. N000140110993, monitored by Drs. L. Patrick Purtell and Ronald D. Joslin.

References

Baggett, J.S., 1998. On the feasibility of merging LES with RANS in the near-wall region of attached turbulent flows. In: Annu. Res. Briefs—1998. Center Turbul. Res., Stanford University, California, pp. 267–277.

Balaras, E., Benocci, C., 1994. Subgrid-scale models in finite-difference simulations of complex wall bounded flows. AGARD CP 551, 2.1.

Balaras, E., Benocci, C., Piomelli, U., 1996. Two-layer approximate boundary conditions for large-eddy simulations. AIAA J. 34, 1111.

Cabot, W.H., 1996. Near-wall models in large-eddy simulations of flow behind a backward-facing step. In: Ann. Res. Briefs—1996. Center Turbul. Res., Stanford University, California, pp. 199–210.

Cabot, W., Moin, P., 2000. Approximate wall boundary conditions in the large-eddy simulation of high Reynolds number flows. Flow Turbul. Comb. 63, 269.

Carati, D., Ghosal, S., Moin, P., 1995. On the representation of backscatter in dynamic localization models. Phys. Fluids 7, 606–616.

Chapman, D.R., 1979. Computational aerodynamics development and outlook. AIAA J. 17, 1293.

Chasnov, J.R., 1991. Simulation of the Kolmogorov inertial subrange using an improved subgrid model. Phys. Fluids A 3, 188–200.

Dean, R.B., 1978. Reynolds number dependence of skin friction and other bulk flow variables in two-dimensional rectangular duct flow. J. Fluids Eng. 100, 215.

Diurno, G.V., Balaras, E., Piomelli, U., 2001. Wall-layer models for LES of separated flows. In: Geurts, B. (Ed.), Modern Simulation Strategies for Turbulent Flows. Philadelphia, RT Edwards, pp. 207–222.

Eswaran, V., Pope, S.B., 1988. Examination of forcing in direct numerical simulations of turbulence. Comput. Fluids 16, 257–278.

Hamba, F., 2002. An approach to hybrid RANS/LES calculation of channel flows. In: Rodi, W., Fueyo, N. (Eds.), Engineering Turbulence Modelling and Experiments, vol. 5. Elsevier, Amsterdam, pp. 297–306.

Leith, C.E., 1990. Stochastic backscatter n a subgrid-scale model: plane shear mixing layer. Phys. Fluids A 2, 297–299.

Mason, P.J., Callen, N.S., 1986. On the magnitude of the subgrid-scale eddy coefficient in large-eddy simulation of turbulent channel flow. J. Fluid Mech. 162, 439–462.

Mason, P.J., Thomson, D.J., 1992. Stochastic backscatter in large-eddy simulation of boundary layers. J. Fluid Mech. 242, 51–78.

Nikitin, N.V., Nicoud, F., Wasistho, B., Squires, K.D., Spalart, P.R., 2000. An approach to wall modeling in large-eddy simulations. Phys. Fluids 12, 1629.

Piomelli, U., Balaras, E., 2002. Wall-layer models for large-eddy simulations. Annu. Rev. Fluid Mech. 34, 349.

Piomelli, U., Balaras, E., Squires, K.D., Spalart, P.R., 2001. Zonal approaches to wall-layer models for large-eddy simulations. AIAA Paper, 2002–3083.

Reynolds, W.C., 1990. In: Lumley, J.L. (Ed.), Whither Turbulence? Turbulence at the Crossroads. Springer-Verlag, Heidelberg, p. 313.

Spalart, P.R., 2000. Strategies for turbulence modeling and simulations. Int. J. Heat Fluid Flow 21, 252–263.

Spalart, P.R., Allmaras, S.R., 1994. A one-equation turbulence model for aerodynamic flows. La Recherche Aérospatiale 1, 5.

Spalart, P.R., Jou, W.H., Strelets, M., Allmaras, S.R., 1997. Comments on the feasibility of LES for wings, and on a hybrid RANS/LES approach. In: Liu, C., Liu, Z. (Eds.), Advances in DNS/LES. Greyden Press, Columbus, pp. 137–148.

Wang, M., Moin, P., 2002. Dynamic wall modeling for large-eddy simulation of complex turbulent flows. Phys. Fluids 14, 2043–2051.